The Role of Large-Scale Eddies in the Climate Equilibrium. Part II: Variable Static Stability

SHUNTAI ZHOU* AND PETER H. STONE

Center for Meteorology and Physical Oceanography, Massachusetts Institute of Technology, Cambridge, Massachusetts

(Manuscript received 10 August 1992, in final form 12 April 1993)

ABSTRACT

Lorenz's two-level model on a sphere is used to investigate how the results of Part I are modified when the interaction of the vertical eddy heat flux and static stability is included. In general, the climate state does not depend very much on whether or not this interaction is included, because the poleward eddy heat transport dominates the eddy forcing of mean temperature and wind fields. However, the climatic sensitivity is significantly affected. Compared to two-level model results with fixed static stability, the poleward eddy heat flux is less sensitive to the meridional temperature gradient and the gradient is more sensitive to the forcing. For example, the logarithmic derivative of the eddy flux with respect to the gradient has a slope that is reduced from ~ 15 on a β-plane with fixed static stability and ~ 6 on a sphere with fixed static stability, to ~ 3 to 4 in the present model. This last result is more in line with analyses from observations. The present model also has a stronger baroclinic adjustment than that in Part I, more like that in two-level β-plane models with fixed static stability, that is, the midlatitude isentropic slope is very insensitive to the forcing, the diabatic heating, and the friction, unless the forcing is very weak.

1. Introduction

Two-level spectral models are powerful tools for studying interactions of large-scale eddies and zonal mean states, if the horizontal resolution is adequate (e.g., Held and Suarez 1978; O'Brien and Branscome 1989; Cehelsky and Tung 1991; Stone and Branscome 1992). These models are more advantageous for process studies than complicated general circulation models (GCMs), because of their greater efficiency. Thus they can be used to carry out many experiments that require long time integrations and many parameter changes. Also, because of their relative simplicity, the results of these models are more easily interpreted and the mechanisms are more easily separated.

In Part I (Zhou and Stone 1993) we presented numerical results from a spherical two-level model with fixed static stability and compared them with the results from a β-plane model (Stone and Branscome 1992, referred to as SB hereafter). The results shed light on the importance of spherical geometry, as well as interactions of the tropical atmosphere with the mid-high-latitude atmosphere. For an eddy regime like the earth's midlatitude atmosphere the differences between the spherical model and the β-plane model are more quantitative than qualitative. This is because spherical geometry mainly affects the eddy momentum flux, and we know from observations (Oort 1971; Edmon et al. 1980) and the model results that the eddy heat flux dominates the eddy forcing of mean states when diabatic heating is realistically strong.

In models with fixed static stability the role of the vertical eddy heat flux is excluded. Models that omit the interaction of this flux with the static stability may be missing an important part of the atmospheric physics. Based upon a highly simplified model and the Charney-Stern theorem, Gutowski (1985) has shown that the observed midlatitude temperature profiles can be understood in terms of such a mechanism. Held and Suarez (1978) calculated explicitly the vertical eddy heat flux and its effect on the static stability using a two-level primitive equation model. They found that the static stability in midlatitudes was maintained mainly by the vertical eddy heat transport and diabatic heating processes. In a further study with the same model, Held (1978a) found that the static stability played an important role in the sensitivity of climate to changes in the solar constant.

However, the model used by Held and Suarez (1978) and Held (1978a) employs a moist adiabatic adjustment parameterization of moist convection. This parameterization is known to give a poor simulation of the interaction between moist convection and large-scale motions (Arakawa and Chen 1987). In particular, when simulations using it are compared to simulations

* Current affiliation: Atmospheric and Environmental Research, Inc., Cambridge, Massachusetts.

Corresponding author address: Dr. Peter H. Stone, Center for Meteorology and Physical Oceanography, Massachusetts Institute of Technology, Cambridge, MA 02139.

with a more realistic penetrative convection scheme, the convective heat transport is substantially less than that with the more realistic scheme, and the vertical eddy heat fluxes by the large-scale motions are much larger (Stone and Yao 1991). Thus it is not clear whether the Held and Suarez (1978) and Held (1978a) results are realistic or robust. In addition, no studies have investigated the role of the vertical eddy heat flux from the point of view of the total eddy forcing of mean states. Indeed, the standard paradigm for discussing the eddy forcing is the nonacceleration theorem of Charney and Drazin (1961), which neglects any explicit forcing by the vertical eddy heat flux.

Thus in this paper we extend our investigation in Part I to include the interaction of large-scale eddies with the vertical temperature structure. The model we use is Lorenz's two-level model (Lorenz 1960) on the sphere, which allows for a variable static stability. It also has a more accurate formulation of the thermodynamic equation than other two-level models (Hollingsworth 1975). We carry out a series of experiments similar to those in Part I and in SB, and compare the results with those previously obtained from fixed static stability experiments.

The paper is organized as follows: in section 2 we describe the model briefly (more details may be found in Part I). In section 3 we study the interactions of the vertical eddy heat flux and static stability and their effect on the equilibrium state. In section 4 we examine the effects of changing external parameters, particularly the diabatic forcing. Finally, in section 5, a summary and conclusions are given.

2. Model description

The model we use is a two-level model on a sphere with no topography. The vorticity equations are exactly the same as those given in Part I. However, the thermodynamic equation is written at the two levels instead of at the interface. The vertical mean of the potential temperature, θ, is represented by $\bar{\theta} = (\theta_1 + \theta_3)/2$, while the static stability is represented by $\hat{\theta} = (\theta_1 - \theta_3)/2$, where the subscripts denote vertical levels. As shown in Part I, there is little difference between using the linear or nonlinear balance equation approximation in simulating the midlatitude eddy regime. Therefore, we use the linear balance equation approximation. Instead of using $\bar{\theta}$, we use $\hat{\Phi} = \frac{1}{2}(\Phi_1 - \Phi_3)$, where Φ is the geopotential, to represent vertical mean temperature. The basic equations are written in nondimensional form as:

$$\frac{\partial}{\partial t}\nabla^2\bar{\psi} = J(\bar{\psi}, \nabla^2\bar{\psi}) - J(\hat{\psi}, \nabla^2\hat{\psi}) - 2\frac{\partial\bar{\psi}}{\partial\lambda} + \bar{\mathcal{D}}, \quad (1)$$

$$\frac{\partial}{\partial t}\nabla^2\hat{\psi} = -J(\bar{\psi}, \nabla^2\hat{\psi}) - J(\hat{\psi}, \nabla^2\bar{\psi}) - 2\frac{\partial\hat{\psi}}{\partial\lambda} - 2\nabla\cdot(\mu\nabla\hat{\varphi}) + \hat{\mathcal{D}}, \quad (2)$$

$$\frac{\partial\hat{\Phi}}{\partial t} = -J(\bar{\psi}, \hat{\Phi}) - J(\hat{\psi}, \bar{\theta}) - \nabla\cdot(\bar{\theta}\nabla\hat{\varphi}) + \bar{\mathcal{Q}}, \quad (3)$$

$$\frac{\partial\hat{\theta}}{\partial t} = -J(\bar{\psi}, \hat{\theta}) - J(\hat{\psi}, \bar{\Phi}) - \nabla\hat{\Phi}\cdot\nabla\hat{\varphi} + \hat{\mathcal{Q}}, \quad (4)$$

$$\nabla^2\hat{\Phi} = 2\nabla\cdot(\mu\nabla\hat{\psi}), \quad (5)$$

where ψ is streamfunction, φ is velocity potential, t is time, λ is longitude, μ is cosine of colatitude, and J is the Jacobian operator. The continuity equation has been used to eliminate the vertical velocity; ψ and φ have been nondimensionalized by Ωa^2, Φ by $\Omega^2 a^2$, and $\hat{\theta}$ by $gH/2\Omega^2 a^2\bar{\theta}_0$, where Ω is the angular velocity, a the radius of the earth, g the acceleration of gravity, H the scale height, and $\bar{\theta}_0$ the global-mean potential temperature.

As in Part I, we represent ψ, φ, Φ, and $\hat{\theta}$ in terms of spherical harmonics and transform Eqs. (1)–(5) into spectral form. We assume that ψ is antisymmetric about the equator and other variables are symmetric, that is, we consider only regimes in which the forcing is symmetric about the equator. In order to determine an appropriate truncation and fundamental wavenumber, we carried out a series of resolution experiments like those in Part I. We found again that five zonal waves with fundamental wavenumber 3 and five meridional modes on a hemisphere, that is, a resolution of 5 $\times$ 5(3), is adequate and efficient for most of the experiments.

Here, $\mathcal{D}$ and $\mathcal{Q}$ denote friction and diabatic heating. The temperature at both levels is driven by a pole-to-equator temperature difference, ΔT_E, in a Newtonian cooling representation of $\mathcal{Q}$. Friction on the lower surface is incorporated by a surface drag. Vertical mixing of horizontal momentum is also included using a latitude-dependent interfacial stress that is negligible outside the tropics (cf. Part I). The external parameters have the same standard values as in Part I, that is,

$$\Delta T_E = 48 \text{ K}, \quad \tau_h = 20 \text{ days},$$

$$\tau_s = 5 \text{ days}, \quad H = 7.4 \text{ km},$$

where τ_h and τ_s are time scales for the Newtonian cooling and surface drag, respectively.

Because we use zonally symmetric forcing in this model, further simplification can be made by assuming that the static stability is also zonally symmetric, that is,

$$\hat{\theta} = \hat{\theta}(t, \mu) = \hat{\theta}_0(t) + \sum_\alpha \hat{\theta}_\alpha(t)P_\alpha(\mu), \quad (6)$$

where $\hat{\theta}_0(t)$ is the global-mean static stability, $\hat{\theta}_\alpha(t)$ is the amplitude of a meridional mode, and P_α is the Legendre function. Unlike the global-mean tempera-

ture, T_0, which does not interact with the eddies and remains constant, $\hat{\theta}_0(t)$ interacts with the vertical eddy heat flux and can play an important role in the dynamics (Held and Suarez 1978). The simplified static stability equation becomes

$$\frac{\partial[\hat{\theta}]}{\partial t} = -[J(\hat{\psi}, \hat{\Phi})] - [\nabla\hat{\Phi}\cdot\nabla\hat{\varphi}] + [\hat{Q}], \quad (7)$$

where the square brackets indicate a zonal mean. This simplification greatly reduces the computation time while having little effect on the budget of static stability.

The diabatic forcing of static stability also has a Newtonian cooling form, that is,

$$\hat{Q} = \alpha(\hat{\theta}_E - \hat{\theta}), \quad (8)$$

where $\alpha = 1/\tau_h$. Similar to ΔT_E, $\hat{\theta}_E$ can be regarded as the static stability in the radiative equilibrium state or in the radiative–convective equilibrium state. For instance, Bryan (1959) simply assumed that $\hat{\theta}_E = 0$, which means that the equilibrium atmosphere always remains at a dry neutral state. Alternatively, $\hat{\theta}_E$ can be calculated from various models, simple or sophisticated. For instance, the temperature structures in radiative–convective equilibrium have been calculated by integrating in time the thermodynamic equations with an explicit forcing, such as radiative fluxes, boundary fluxes, and convective adjustment, until a steady state was achieved (Held and Suarez 1978; Eliasen 1982). Because the explicit forcing was parameterized in different ways, the equilibrium states also differed. Nevertheless, common features are shown by these calculations, and they seem to be physically meaningful, for example, the atmosphere is more stable in high latitudes than in low latitudes; the radiative–convective equilibrium state is more stable than the pure radiative equilibrium state, etc.

For most of our experiments we specify a relatively realistic $\hat{\theta}_E$, which is shown in Fig. 1. It was obtained from a numerical experiment with the GISS zonal-mean statistical–dynamical model (Stone and Yao 1990). In this experiment, the lower boundary was an ocean with the observed zonal-mean sea surface temperature; the equilibrium state was calculated for January conditions by incorporating all dynamical processes except for the large-scale vertical eddy heat transports. A mean equilibrium static stability was then calculated by averaging the Northern and Southern hemispheric values. Since the vertical heat transport by the zonal-mean circulations is very small (Stone and Yao 1991), this equilibrium static stability corresponds to that in radiative–convective equilibrium. This equilibrium static stability, shown in Fig. 1, has a relatively uniform meridional structure, but with larger values near the pole. Since the moist convection parameterization in the GISS model is a penetrative convection scheme (Yao and Stone 1987), the static stability in the radiative–convective equilibrium state is about twice that in the moist model used by Held and Suarez (1978). This larger stability will tend to suppress the baroclinic instability and eddy heat fluxes in our model compared to theirs. Thus our results will supply a good test of how robust their results are.

3. The role of the vertical eddy heat flux

a. *The climate equilibrium*

The equilibrium static stability calculated using our standard values for the parameters is shown in Fig. 1. Compared with the specified forcing state (radiative–convective equilibrium state), the global-mean static stability has increased appreciably, with the biggest increase being in midlatitudes. These features are very similar to those found by Held and Suarez (1978). The calculated mean static stability in midlatitudes is in fact close to the standard value we chose for our fixed static stability experiments in Part I, $\hat{\theta} = 23.8$ K. (This value corresponds to $\Gamma_0 = 0.013$ in the notation of Part I, and a Brunt–Väisälä frequency of 10^{-2} s^{-1}.) Between 30° and 60°, for example, the mean static stability is 23.3 K.

Since the external parameters had the same standard values in Part I, we can compare the results in the standard runs from Parts I and II to see if the *variability* of the static stability affects the climate equilibrium. In fact, the statistical equilibrium states of the zonal flow, the meridional wind, the temperature, and the mean meridional circulation (MMC) streamfunction are quite similar in the two cases. Thus we do not show the results for these fields with variable static stability. Even quantitatively the differences in midlatitudes are small. For example, with variable static stability the meridional temperature gradient at 45° is 7% less, the peak value of the meridional eddy flux is 10% greater,

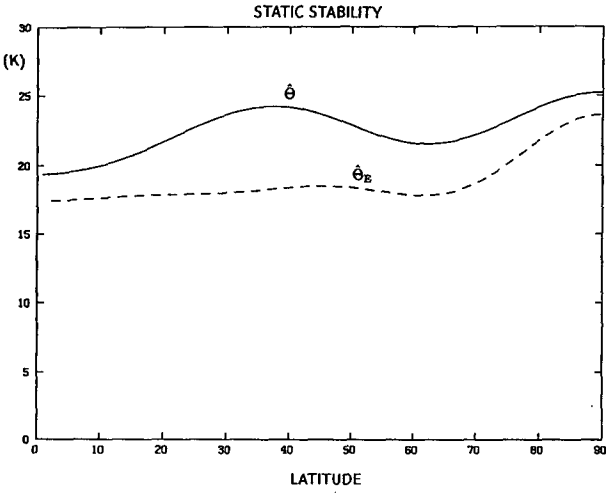

FIG. 1. The calculated static stability, $\hat{\theta}$ (solid), and the static stability in radiative–convective equilibrium, $\hat{\theta}_E$ (dashed).

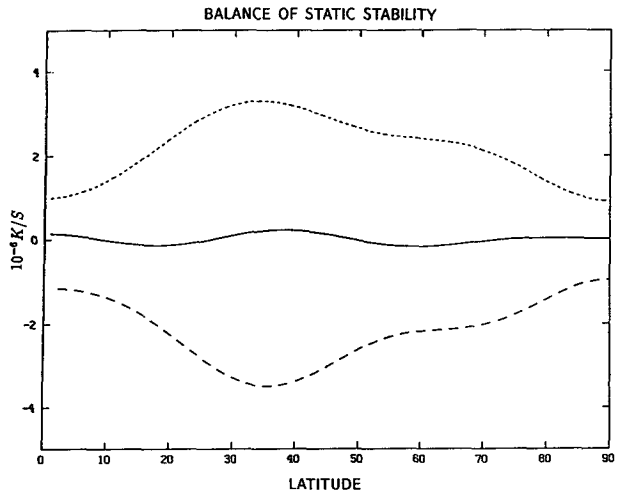

FIG. 2. The budget of static stability: the solid line is the temperature advection by the nondivergent eddy winds; the dotted line is the temperature advection by all divergent motions (eddies and MMC); the dashed line is the diabatic forcing.

and the peak value of the meridional eddy momentum flux is 4% greater. We can conclude that, to a first approximation, the variability of the static stability does not affect the climate equilibrium. Thus it would be feasible to simulate the climate equilibrium by using a dynamical model with fixed static stability coupled to a separate model for the maintenance of the mean static stability.

b. *The budget of static stability*

The static stability balance is maintained by three different physical processes, that is,

$$[J(\hat{\psi}, \hat{\Phi})] + [\nabla\hat{\Phi}\cdot\nabla\hat{\varphi}] - [\hat{Q}] = 0. \qquad (9)$$

The first term represents the temperature advection by the nondivergent component of the eddy winds; the second term is the temperature advection by all divergent motions (eddies and MMC); the last term denotes the diabatic forcing of the static stability. It should be pointed out that the first term would vanish if the quasigeostrophic approximation were used. As shown in Fig. 2, this term is relatively small compared to the other terms. Therefore, the balance of static stability is primarily between the divergent wind term and the diabatic term. The divergent wind transport tends to increase the static stability in all latitudes, with a peak in the subtropics rather than in midlatitudes. The diabatic heating term tends to decrease the static stability.

The divergent wind heat transport can be further decomposed into three parts, that is,

$$[\nabla\hat{\Phi}\cdot\nabla\hat{\varphi}] = \nabla[\hat{\Phi}]\cdot\nabla[\hat{\varphi}] + [\nabla\cdot(\hat{\Phi}^*\nabla\hat{\varphi}^*)] - [\hat{\Phi}^*\nabla^2\hat{\varphi}^*], \qquad (10)$$

where the asterisk indicates a deviation from the zonal mean. The first term on the right-hand side of Eq. (10) represents the heat transport by the MMC; the second term represents the meridional heat transport by (divergent) eddies; the third term represents the vertical heat transport by eddies.

The characteristics of the divergent wind terms are shown in Fig. 3. First, we note that the vertical eddy heat transport dominates in mid- to high latitudes. This feature is similar to Held and Suarez's (1978) results. In addition, we note that the MMC heat transport is almost perfectly out of phase with the vertical eddy heat transport. The direct Hadley cell tends to increase the static stability in low latitudes, while the indirect Ferrel cell tends to decrease the static stability in midlatitudes. The role of the MMC in the maintenance of static stability is similar to its role in the maintenance of the meridional temperature gradient. In other words, the MMC heat transports tend to counteract the eddy heat transports. We also note that the meridional heat transports by divergent eddies are small and out of phase with the transports by nondivergent eddies (Fig. 2). Thus the total meridional eddy heat transport is negligible in the balance of the static stability.

c. *Sensitivity to* $\hat{\theta}_E$

The budget of static stability is clearly dependent on the forcing of static stability, $\hat{\theta}_E$. To examine the effect of changes of $\hat{\theta}_E$, we consider a different $\hat{\theta}_E$, corresponding to a pure radiative equilibrium static stability. We used a simple earth–atmosphere coupled model (Saltzman 1968; Wiin-Nielson 1970) to calculate this $\hat{\theta}_E$, which is shown in Fig. 4. The equilibrium tropical atmosphere is now much less stable than the midlatitude atmosphere, due to the absence of convective adjustment. This $\hat{\theta}_E$ gives a sharp contrast to the $\hat{\theta}_E$ in

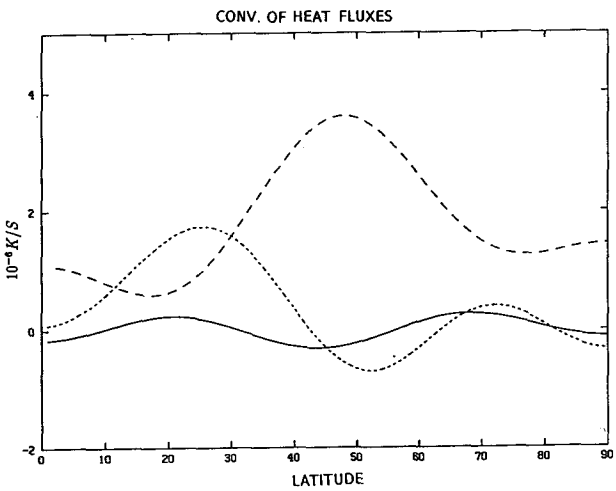

FIG. 3. The components of heat flux convergence by divergent motions: meridional eddy flux (solid), vertical eddy flux (dashed), and MMC flux (dotted).

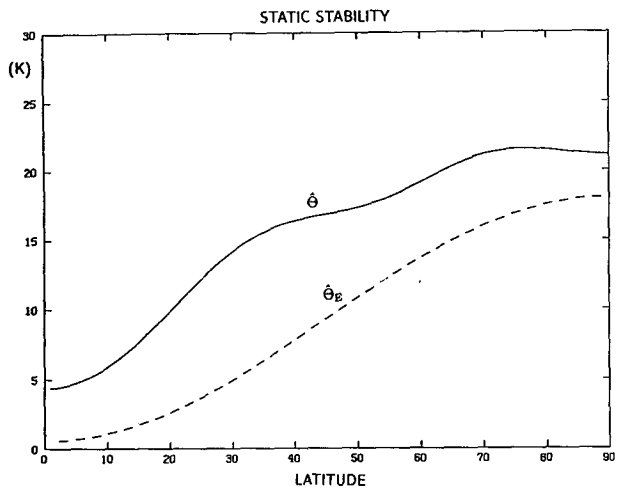

FIG. 4. Same as Fig. 1 except that $\hat{\theta}_E$ is the static stability in radiative equilibrium.

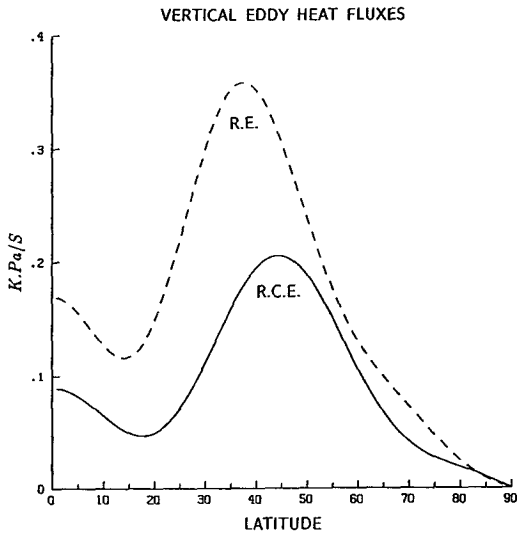

FIG. 5. Vertical eddy heat fluxes calculated using two choices for $\hat{\theta}_E$. The solid line is for radiative–convective equilibrium, and the dashed line is for radiative equilibrium.

the radiative–convective equilibrium. We carried out an experiment with this different $\hat{\theta}_E$, but all other external parameters unchanged.

Compared with the previous experiment, the equilibrium general circulation and meridional temperature structure showed only small differences. In particular, the meridional eddy heat transport was not sensitive to the change in $\hat{\theta}_E$. However, the vertical eddy heat transport and its impact on the static stability are very sensitive to $\hat{\theta}_E$. The calculated static stability is shown in Fig. 4. The increase of the mean static stability in midlatitudes from the radiative equilibrium state is as much as 100%, in contrast to the increase from the radiative–convective equilibrium, which was $\leqslant$30%. The vertical eddy heat flux is shown in Fig. 5. It is about twice as large when the equilibrium state is the pure radiative state. However, the meridional structure of the vertical eddy heat flux is hardly changed by changing $\hat{\theta}_E$.

d. Relative importance of the vertical eddy heat flux

In SB and Part I, the forcing of the time- and zonal-mean temperature fields by the meridional eddy fluxes of heat and momentum was evaluated by calculating the contributions of each eddy flux to the divergence of the Eliassen–Palm (EP) flux. The forcing by the eddy momentum flux is larger on the sphere than on the β plane, but the forcing by the eddy heat flux is not much different and dominates in both cases. We cannot extend this comparison to include the vertical eddy heat flux because the nonacceleration theorem is based on approximations that exclude the effect of this eddy flux a priori.

Instead we evaluate the impact of the three eddy fluxes on the temperature field by calculating the heating rates associate with each flux. An appropriate heating rate to associate with the eddy momentum flux is that due to the MMC heat transport. This follows from the observation that in two-level quasigeostrophic models the relative contribution of the eddy momentum flux to the divergence of the EP flux is given precisely by the ratio of the MMC heat transport to the meridional eddy heat transport (SB).

Table 1 shows the peak values of the heating rates in equilibrium due to each of the three heat fluxes along with the latitudes where the peak values occurred. Included are values from both experiments with the two different choices for $\hat{\theta}_E$ described above. The heating rates make the meridional eddy momentum flux look more important, relative to the meridional eddy heat flux, than their contributions to the divergence of the EP flux, because the meridional scale of the Ferrel cell and of the MMC heat transport is smaller than that of the eddy heat flux. Nevertheless, the effect of the eddy heat flux is still dominant when measured by the heating rates. In addition, Table 1 shows that the forcing by the vertical eddy heat flux is by no means negligible. In the most realistic experiment, the one with variable static stability and $\hat{\theta}_E$ corresponding to radiative–convective equilibrium, the heating rate associated with

TABLE 1. Peak heating rates (and location), 10^{-6} K s^{-1}.

	Meridional eddy heat flux	MMC heat flux	Vertical eddy heat flux
$\hat{\theta}_E$ in radiative–convective equilibrium	6.2 (69°)	4.5 (37°)	3.6 (48°)
$\hat{\theta}_E$ in radiative equilibrium	6.0 (70°)	2.7 (33°)	5.6 (40°)

the vertical eddy heat flux is smaller than the other two heating rates but is still 58% as large as the largest heating rate. This suggests that models that neglect this eddy flux, or specify the static stability, for example, quasigeostrophic models, are not well suited to studying *changes* in the heat balance and climate, even if the climate itself is not much affected. Indeed, we will see in the next section that the impact of the vertical eddy heat flux has a significant effect on climate sensitivity.

4. Climate sensitivity

a. Parameter experiments

We have carried out a series of experiments to determine the effects of changes in external parameters. These experiments are similar to those in Part I except that the static stability is no longer an external parameter. The general results are summarized in Table 2, which shows equilibrium values of quantities that characterize the climate and general circulation from three different series of experiments. In each series a single external parameter was varied, as indicated in the first column of the table, while the other parameters were held fixed at their standard values. All the experiments used the $\hat{\theta}_E$ corresponding to radiative–convective equilibrium. For comparison with the results from the experiments, we note that in radiative–convective equilibrium $\delta T = 0.342\Delta T_E$ and $\hat{\theta}_0 = 18.1$ K.

Most of the effects of changes in ΔT_E, τ_h, and τ_s are qualitatively similar to the effects found with fixed static stability (cf. Table 3 of part I). In general, when diabatic heating increases (ΔT_E increases or τ_h decreases) the temperature gradient, winds, and all the eddy transports increase. On the other hand changes in τ_s mainly affect the eddy momentum flux and surface zonal wind, while leaving the temperature structure and eddy heat fluxes largely unchanged.

One major difference from the earlier results involves the parameter R. For a two-level quasigeostrophic model, this parameter measures the degree to which the divergence of the meridional component of the EP flux cancels out the divergence of the vertical component, that is, if $R = 1$ the divergence of the EP flux is zero (SB). With fixed static stability, increases in ΔT_E were accompanied by decreases in R, but with variable static stability they are accompanied by increases in R. This is because in the latter case the static stability increases, and this tends to suppress the vertical component of the EP flux sufficiently that now R increases. Thus the relative importance of the eddy momentum flux in forcing the mean flow *increases* as ΔT_E increases, rather than decreases. The changes in R accompanying changes in τ_h and τ_s are qualitatively similar to those with fixed static stability. In particular, as shown in SB, if τ becomes very large, $R \to 1$, and there is no quasigeostrophic eddy forcing of the mean flow.

Table 2 also illustrates the sensitivity of the static stability to the external parameters. When ΔT_E increases, the forcing for the static stability is unchanged, but the forcing for the meridional temperature gradient increases. Thus the eddy activity and the vertical eddy heat flux increase. The latter effect causes the static stability to increase. When τ_h decreases, the forcing for

TABLE 2. Characteristic quantities in the parameter experiments.

		δT	$\hat{\theta}_0$	$\hat{\theta}_{45°}$	$[v]_l$	$[u]_s$	$[\overline{u^*v^*}]_l$	$[\overline{v^*T^*}]_l$	$[\overline{\omega^*T^*}]_l$	R
$\Delta T_E =$	30 K	10.0	18.9	19.7	.16	4.9	3.3	2.45	0.07	.30
	48 K	13.1	21.6	23.2	.27	12.6	7.5	6.85	0.21	.30
	72 K	16.5	26.4	28.7	.42	19.4	13.7	14.3	0.45	.33
	144 K	28.3	42.6	46.6	.68	36.8	26.4	35.8	1.26	.37
$\tau_h =$	5 days	14.4	19.8	20.6	.53	18.9	12.6	13.5	0.37	.24
	20 days	13.1	21.6	23.2	.27	12.6	7.5	6.85	0.21	.30
	80 days	11.9	23.2	26.1	.16	6.6	3.3	2.69	0.07	.35
$\tau_s =$	2.5 days	13.4	21.5	23.0	.28	8.0	8.9	6.60	0.20	.33
	5 days	13.1	21.6	23.2	.27	12.6	7.5	6.85	0.21	.30
	10 days	12.5	21.5	23.7	.24	19.5	6.6	6.39	0.19	.30
	20 days	13.0	21.5	23.8	.24	28.6	5.2	6.19	0.19	.28

u zonal wind
v meridional wind
δT $[\bar{T}_{35°}-\bar{T}_{55°}]$ (K)
$\hat{\theta}_0$ global mean value of $\hat{\theta}$ (K)
$\hat{\theta}_{45°}$ $\hat{\theta}$ at 45° (K)
$[v]_l$ the maximum $[v]$ at the upper level (m s^{-1})
$[u]_s$ the maximum $[u]$ at the surface (m s^{-1})
$[\overline{u^*v^*}]_l$ the peak value of $[\overline{u^*v^*}]\sin^2\theta$, (m^2 s^{-2})
$[\overline{v^*T^*}]_l$ the peak value of $[\overline{v^*T^*}]\sin\theta$, (K m s^{-1})
$[\overline{\omega^*T^*}]_l$ the peak value of $[\overline{\omega^*T^*}]\sin\theta$, (K Pa s^{-1})
R ratio of the peak magnitude of the meridional heat flux by the mean meridional circulation to that by eddies.

both the static stability and the meridional temperature gradient increases. The latter effect again leads to an increase in the vertical eddy heat flux, which tends to increase the static stability. However, the former effect tends to force the static stability nearer to the radiative–convective equilibrium value, that is, it tends to decrease it. This effect dominates, so the static stability decreases when τ_h decreases. However, because the two effects act in opposite directions the static stability is much less sensitive to τ_h than to ΔT_E. Finally, the static stability is very insensitive to changes in the surface friction.

b. *Baroclinic adjustment*

The baroclinity of a system can be represented by the slope of its isentropic surface, α_θ, which is equal to the ratio of the meridional temperature gradient and static stability. Thus,

$$\alpha_\theta \propto \frac{\delta T}{\hat{\theta}} \propto \frac{\hat{U}}{N^2}, \tag{11}$$

where $\hat{U}$ is the zonal-mean vertical shear of the zonal wind and N is the Brunt–Väisälä frequency. According to the baroclinic adjustment hypothesis, baroclinic eddies will maintain the isentropic slope near a constant value (Stone 1978; SB). This implies that the isentropic slope is insensitive to changes in diabatic forcing. In our experiments, when ΔT_E varies, $\hat{U}$ and N^2 vary simultaneously. The resulting relationship in midlatitudes is shown in Fig. 6. The calculated values of $\hat{U}$ are represented by X's, and N^2, instead of ΔT_E, is the abscissa for easier comparison with our earlier results (Fig. 8 of Part I). To help interpret the relationship we also include in Fig. 6 the conventional two-level-model critical shear for baroclinic instability (Phillips 1954) (denoted $\hat{U}_c$, and represented by the dotted line in Fig. 6) and the shear in radiative–convective equilibrium (denoted $\hat{U}_E$, and represented by the solid line in Fig. 6). The dashed line is a straight-line best fit to the calculated values for large shears.

When ΔT_E becomes small, the calculated N^2 approaches a limiting value, N_E^2, which is the static stability of the radiative–convective equilibrium state ($N_E^2 \propto \hat{\theta}_E$); $\hat{U}$ also approaches $\hat{U}_E$. There is a critical value of ΔT_E at which baroclinic instability sets in, about 20 K when the other parameters have their standard values. For smaller values there are no eddies and the temperature structure in middle and high latitudes is that of the radiative–convective equilibrium state (see part I). For larger values of ΔT_E, $\hat{U} \propto N^2$, that is, changes in $\hat{U}$ and N^2 compensate each other in just such a way as to maintain the equilibrium isentropic slope at a fixed value. A closely analogous behavior occurred on the β plane with fixed static stability, that is, changes in N^2 in the eddy regime led to changes in $\hat{U} \propto N^2$, and the isentropic slope was insensitive to ΔT_E (SB). The behavior on the sphere with fixed static stability differed in part. In the eddy regime $\hat{U}$ was again proportional to N^2, but the isentropic slope was much more sensitive to ΔT_E. For example, on the sphere, when ΔT_E increases from 48 to 144 K, with variable static stability α_θ only increases by 8%, but with fixed static stability it increased by 45% (cf. Table 3 of part I). As can be seen from Table 2, α_θ is insensitive to τ_h and τ_s, as was the case on the β plane (SB); α_θ is most sensitive to τ_h, but even in this case the derivative of $\log \alpha_\theta$ with respect to $\log \tau_h$ is only -0.15.

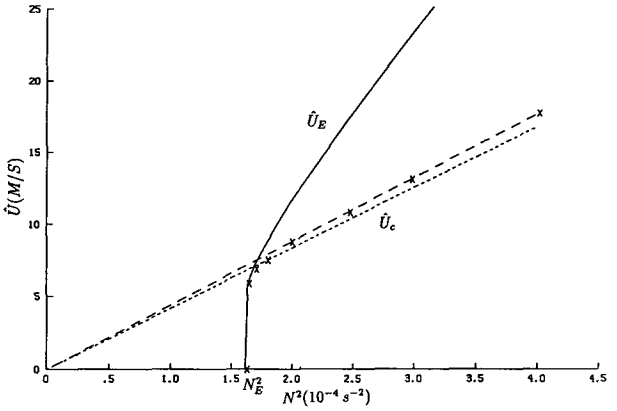

FIG. 6. The vertical shear of the zonal wind at 45° as a function of static stability, N^2. The X's are model results for various choices of ΔT_E; the solid line is the equilibrium vertical shear associated with ΔT_E; the dotted line is Phillips's criterion for baroclinic instability; and the dashed line is the best fit of the calculated points for large shears. (N.B. The Phillips criterion is *not* the stability criterion in the model used here. See text.)

Another interesting feature of our results is that the equilibrium isentropic slope in the eddy regime is very close to the critical value for baroclinic instability in Phillips's (1954) two-level model. This was not the case in Part I, where the slope was typically about twice Phillips's critical value (cf. Fig. 8 of Part I). The sharp contrast of isentropic slopes in the two models is mainly due to the different formulations of the thermodynamic equations, but is also partly due to the effect of the vertical eddy heat flux. In Lorenz's model the thermodynamic equation is better represented since it is evaluated at two levels rather than one. This leads to a critical slope for baroclinic instability that is half that in Phillips's model (Hollingsworth 1975; Arakawa and Moorthi 1988). The fact that the equilibrium shear in the Lorenz model is near the critical value defined in the Phillips's model appears to be a coincidence. The interaction of the static stability with the vertical eddy heat flux by itself only reduces the supercriticality by ~30%. Obviously, our model results are in better agreement with observations (Stone 1978; Stone and Carlson 1979; Mole and James 1990).

In fact, all these features are insensitive to $\hat{\theta}_E$. Figure 7 shows results for a set of experiments identical to those shown in Fig. 6 except that $\hat{\theta}_E$ was assigned the radiative equilibrium values shown in Fig. 4. The be-

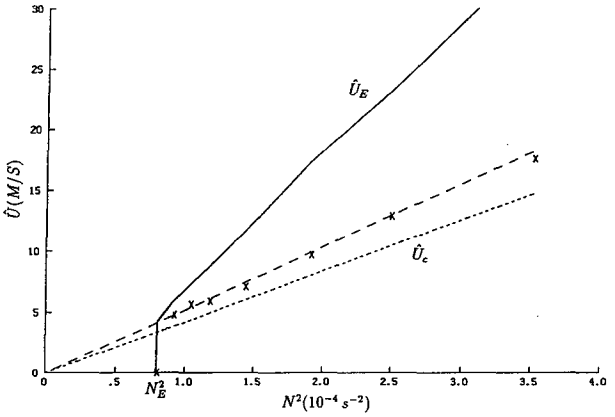

FIG. 7. Same as in Fig. 6 except that $\hat{\theta}_E$ corresponds to radiative equilibrium.

havior is very similar to that shown in Fig. 6, and the isentropic slopes in the eddy regime are only 15% larger, even though $\hat{\theta}_E$ at 45° is only one-half as large. In general the isentropic slopes in the eddy regime are quite insensitive to the equilibrium values that the isentropic slopes would have in the absence of large-scale eddies.

c. *Temperature gradient and eddy heat flux*

Theoretical parameterizations and empirical analyses show a power relationship between the temperature gradient (δT) and the vertically integrated eddy heat flux, T_{ed}, that is, $T_{ed} \propto (\delta T)^n$. If the isentropic slope is a constant, then the theoretical parameterizations predict that $n = 2\frac{1}{2}$ (Stone 1972; Held 1978b; Branscome 1983). Empirical analysis of the seasonal changes in midlatitudes give $n \approx 2$ (Stone and Miller 1980). In SB and Part I we examined the power relationship implied by our results with fixed static stability, and found $n \approx 15$ on the β plane, and $n \approx 6$ on the sphere, both too large compared with observations.

We performed a similar analysis using our present results with variable static stability. Figure 8 shows the eddy heat flux plotted against the meridional temperature gradient. The X's indicate model results for various ΔT_E; δT and T_{ed} are plotted on a logarithmic scale, so that a power relationship between δT and T_{ed} is indicated by a straight line, and the slope of the line is the exponent n. The calculated points of δT and T_{ed} are well aligned for ΔT_E ranging from 30 K to 72 K, but curve down somewhat for larger ΔT_E. The slope, that is, the exponent n, is approximately four for smaller values of ΔT_E, and approximately two for larger values. For our standard parameter choices ($\Delta T_E = 48$ K and $\hat{\theta}_E$ corresponding to radiative–convective equilibrium) $n = 3.4$. This is clearly closer to the empirical result than the earlier results with fixed static stability. The remaining discrepancy may simply be due to the two-level model's crude representation of the vertical structure of the atmosphere. For example, the empirical result $n \approx 2$ is based on *surface* temperature gradients (Stone and Miller 1980), whereas the gradients higher up are considerably smaller (Oort and Peixoto 1983). If we recompute the empirical value of n, using the Northern Hemisphere seasonal changes given by Oort and Peixoto (1983), but calculating T_{ed} and δT in the same way as in the two-level model, that is, just from (interpolated) values at 250 and 750 mb, we find $n \approx 4$.

d. *Zonal spectrum of the eddy heat transport*

In order to determine which zonal wavenumbers transport most of the heat, we calculate the eddy heat transport in the spectral domain. The portions carried by individual wavenumbers vary with ΔT_E. The peak values of the eddy heat fluxes for wavenumbers 3, 6, 9, and total heat flux are shown in Fig. 9b as a function ΔT_E. For comparison, the results calculated from the model with fixed static stability are also shown (Fig. 9a). In general, the spectral features are very similar to those found in a β-plane model with fixed static stability by Cehelsky and Tung (1991). When ΔT_E is small, both wavenumbers 3 and 6 are responsible for most of the heat transport. The transport by wavenumber 9 is relatively small, and the contribution by higher wavenumbers is negligible. When ΔT_E increases, the portion of heat transported by wavenumber 3 becomes dominant. We note that the smaller exponent in the T_{ed}, δT relation appears to be associated with the regime where wavenumber 3 dominates the heat transport.

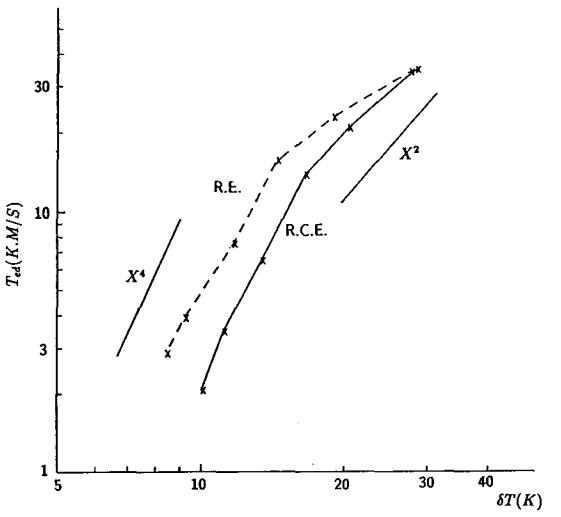

FIG. 8. The eddy heat flux as a function of the temperature gradient in midlatitudes. The X's are the model results for ΔT_E = 30, 36, 48, 72, 96, and 144 K from bottom to top. The dashed line denotes the results with $\hat{\theta}_E$ chosen to be in radiative equilibrium and the solid line the results with $\hat{\theta}_E$ based on radiative–convective equilibrium.

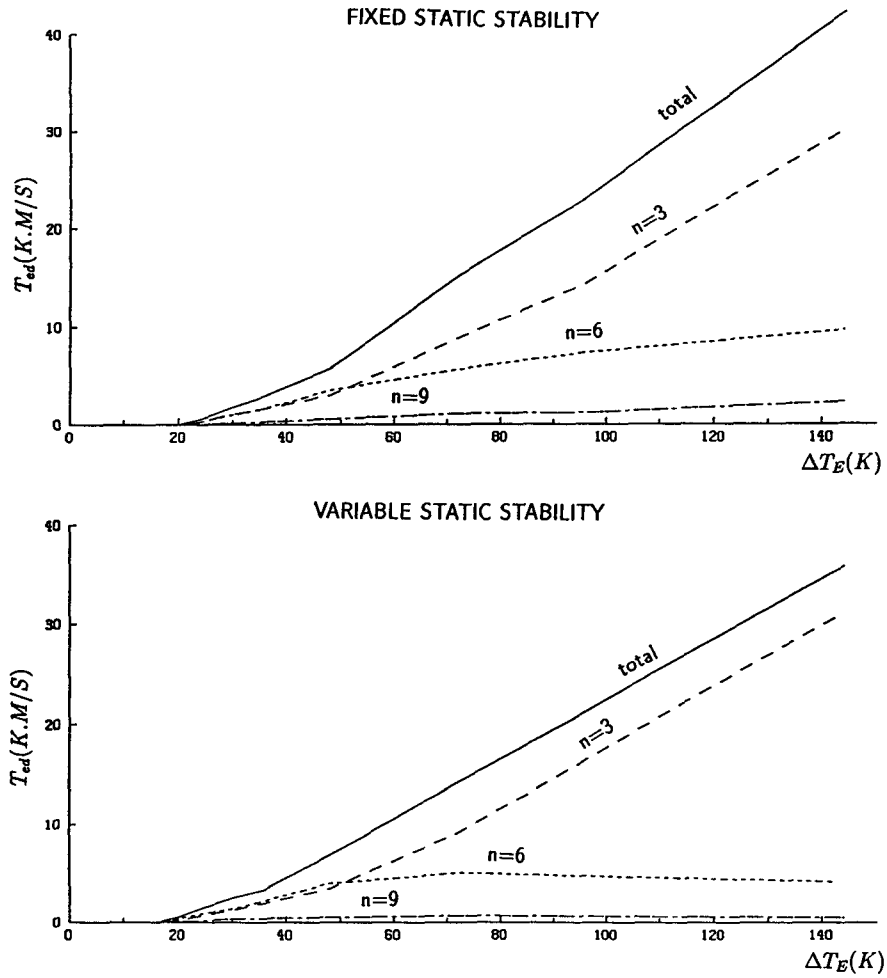

FIG. 9. The peak values of eddy heat flux by individual wavenumbers as a function of ΔT_E. (a) Fixed static stability; (b) variable static stability. The solid line is for all wavenumbers, the dashed, dotted, and dot-dashed lines are for wavenumbers 3, 6, and 9, respectively.

Cehelsky and Tung explain the behavior for large ΔT_E as being due to energy cascades to the longest wave through nonlinear wave–wave interactions. When the forcing increases, the heat transport by the most unstable wave (near wavenumber 6) becomes saturated, and the longest wave present becomes the wave mainly responsible for the required heat transport. The upscale energy cascade mechanism seems to be more effective in our spherical model with variable static stability. For example, when ΔT_E increases, the portion of the eddy heat flux carried by wavenumbers 6 and 9 becomes relatively smaller. In particular, these short wave fluxes exhibit a behavior different from that with fixed static stability. They increase with ΔT_E initially but halt at some turning point ($\sim$72 K) and decrease slightly for larger ΔT_E. In the case with fixed static stability, these fluxes increase with ΔT_E monotonically.

It should be pointed out that energy cascade is not the only mechanism for explaining the fact that the longest wave transports the most heat. The amount of heat transport also depends on the phase correlation between v^* and T^*. Although our model results show that the longest wave (wavenumber 3) is dominant in the spectrum of eddy kinetic energy for large ΔT_E, this might be because wavenumbers 1 and 2 are omitted in the model. To clarify this point, we have carried out an experiment in which the fundamental wavenumber is 1, all zonal wavenumbers $\leqslant$ 15 are retained, and ΔT_E = 96 K, with the other parameters set the same as before. We found that wavenumber 1 does have the largest amount of eddy kinetic energy, due to the upscale cascade mechanism. However, the dominant heat-transporting wave is wavenumber 4, with wavenumber 3 being the second most important. It seems that, for large ΔT_E, the most efficient wavenumbers in transporting heat are between the most unstable wave (wavenumber 5 in our model according to linear instability analysis) and the longest wave. Of course, it is possible that for even larger values of ΔT_E than we

have examined, the waves with the most heat transport might shift to even larger scales.

5. Summary and discussion

Our results confirm the results of Held and Suarez (1978) about the importance of the vertical eddy heat flux in two-level models on a sphere. This is in spite of the substantial differences between our models, particularly the different static stability of the radiative–convective equilibrium states. We note that there are other substantial differences in the models as well. For example, their model included detailed radiative transfer calculations, a hydrological cycle, and an interactive moist convection calculation. Nevertheless, in both models the vertical eddy heat flux causes a significant increase in the static stability in midlatitudes, with $\hat{\theta}$ increasing by $\sim$6 K, corresponding to a decrease of $\sim 1\frac{1}{2}$ K/km in the lapse rate. Also the associated heating rates are $\sim$0.4 K/day in both models. These heating rates are comparable to those associated with the meridional heat transports by eddies and by the zonal-mean meridional wind.

We have also used our model to study how the interaction of the vertical eddy heat flux with the static stability affects the sensitivity of temperature structure to changes in the forcing. We found that it considerably strengthens the baroclinic adjustment in the spherical model, making the isentropic slopes very insensitive to ΔT_E, that is, to the differential heating. We note that the β-plane model with fixed static stability has a similar behavior (SB), but this appears to be something of a coincidence, resulting from two offsetting deficiencies. First, the meridional eddy heat flux on the β plane is much more sensitive to the differential heating than on the sphere, making it difficult to change the meridional temperature gradient. Second, because of the omission of the vertical eddy flux–static stability interaction, the static stability is fixed. The net result is that the isentropic slopes in the eddy regimes of conventional quasigeostrophic β-plane models are also very insensitive to the differential heating. By contrast, on the sphere, with interactive static stability, the meridional eddy heat flux is much less sensitive to the differential heating. Thus the meridional temperature gradient is much more sensitive to the differential heating, but changes in the static stability offset these changes, so that the isentropic slope is again preserved.

The sensitivity of the meridional eddy flux can be measured by the exponent in the relation $T_{ed} \sim (\delta T)^n$ and in our model in midlatitudes, for realistic parameter values, $n \sim 3$ to 4, whereas in the β-plane model with fixed static stability $n \sim 15$. Another interesting effect of the interaction between the eddies and the static stability is that it causes the relative importance of the forcing of the zonal-mean zonal wind and temperature fields by the eddy momentum flux to increase as the differential heating increases, rather than decrease.

These results together with the results of Part I demonstrate the importance of both spherical geometry and an interactive static stability in determining the sensitivity of the climate and general circulation to changes in forcing. Without including these effects it is not possible to simulate accurately how both the meridional temperature structure and the isentropic slopes in midlatitudes respond to changes in forcing. Of course the model we have used in this paper is still a very idealized model of the real atmosphere. We note in particular that both our model and the model used by Held and Suarez (1978) and Held (1978) represent the vertical structure of the atmosphere very crudely because of their two-level approximation. It remains to be determined to what extent our results will carry over to a model with much better vertical resolution.

Acknowledgments. This work was supported by the National Science Foundation under Grant ATM-8803466 and by the NASA Goddard Space Flight Center under Grant NGR 22-009-727.

REFERENCES

Arakawa, A., and J.-M. Chen, 1987: Closure assumptions in the cumulus parameterization problem. *J. Meteor. Soc. Japan* (Suppl.), 107–131.

——, and S. Moorthi, 1988: Baroclinic instability in vertical discrete systems. *J. Atmos. Sci.*, **45**, 1600–1707.

Branscome, L. E., 1983: A parameterization of transient eddy heat flux on a beta-plane. *J. Atmos. Sci.*, **40**, 2508–2521.

Bryan, K., 1959: A numerical investigation of certain features of the general circulation. *Tellus*, **11**, 163–173.

Cehelsky, P., and K. K. Tung, 1991: Nonlinear baroclinic adjustment. *J. Atmos. Sci.*, **48**, 1930–1947.

Charney, J. G., and P. G. Drazin, 1961: Propagation of planetary scale disturbances from the lower into the upper atmosphere. *J. Geophys. Res.*, **66**, 83–109.

Edmon, H. J., B. J. Hoskins, and M. E. McIntyre, 1980: Eliassen–Palm cross-sections for the troposphere. *J. Atmos. Sci.*, **37**, 2600–2616.

Eliasen, E., 1982: Climate modeling using an equivalent meridional circulation. *Tellus*, **34**, 228–244.

Gutowski, W. J., 1985: A simple model for the interaction between vertical eddy heat fluxes and static stability. *J. Atmos. Sci.*, **42**, 346–358.

Held, I. M., 1978a: The tropospheric lapse rate and climatic sensitivity: Experiments with a two-level atmospheric model. *J. Atmos. Sci.*, **35**, 2083–2098.

——, 1978b: The vertical scale of an unstable baroclinic wave and its importance for eddy heat flux parameterizations. *J. Atmos. Sci.*, **35**, 572–576.

——, and M. J. Suarez, 1978: A two-level primitive equation atmospheric model designed for climatic sensitivity experiments. *J. Atmos. Sci.*, **35**, 206–229.

Hollingsworth, A., 1975: Baroclinic instability of a simple flow on the sphere. *Quart. J. Roy. Meteor. Soc.*, **101**, 495–528.

Lorenz, E. N., 1960: Energy and numerical weather prediction. *Tellus*, **12**, 364–373.

Mole, N., and I. N. James, 1990: Baroclinic adjustment in a zonally varying flow. *Quart. J. Roy. Meteor. Soc.*, **116**, 247–268.

O'Brien, E., and L. Branscome, 1989: Minimal modeling of the extratropical general circulation. *Tellus*, **41A**, 292–307.

Oort, A. H., 1971: The observed annual cycle in the meridional transport of atmospheric energy. *J. Atmos. Sci.*, **28**, 325–339.

——, and J. P. Peixoto, 1983: Global angular momentum and energy balance requirements from observations. *Advances in Geophysics,* Vol. 25, Academic Press, 355–490.

Phillips, N. A., 1954: Energy transformation and meridional circulations associated with simple baroclinic waves in a two-level quasi-geostrophic model. *Tellus,* **6,** 273–286.

Saltzman, B., 1968: Steady state solutions for axially-symmetric climatic variables. *Pure Appl. Geophys.,* **69,** 237–259.

Stone, P. H., 1972: A simplified radiative–dynamical model for the static stability of rotating atmospheres. *J. Atmos. Sci.,* **29,** 405–418.

——, 1978: Baroclinic adjustment. *J. Atmos. Sci.,* **35,** 561–571.

——, and J. H. Carlson, 1979: Atmospheric lapse rate regimes and their parameterization. *J. Atmos. Sci.,* **36,** 415–423.

——, and D. A. Miller, 1980: Empirical relations between seasonal changes in meridional temperature gradients and meridional fluxes of heat. *J. Atmos. Sci.,* **37,** 1708–1721.

——, and M. Yao, 1990: Development of a two-dimensional zonally averaged statistical-dynamical model. Part III: The parameterization of the eddy fluxes of heat and moisture. *J. Climate,* **3,** 726–740.

——, and ——, 1991: Vertical eddy heat fluxes from model simulations. *J. Climate,* **4,** 304–317.

——, and L. Branscome, 1992: Diabatically forced nearly inviscid eddy regimes. *J. Atmos. Sci.,* **49,** 355–367.

Wiin-Nielson, A., 1970: A theoretical study of the annual variation of atmospheric energy. *Tellus,* **22,** 1–15.

Yao, M.-S., and P. H. Stone, 1987: Development of a two-dimensional zonally averaged statistical-dynamical model. Part I: The parameterization of moist convection and its role in the general circulation. *J. Atmos. Sci.,* **44,** 65–82.

Zhou, S., and P. H. Stone, 1993: The role of large-scale eddies in the climate equilibrium, Part I: Fixed static stability. *J. Climate,* **6,** 985–1001.